



Supplement of

Atmospheric evolution of environmentally persistent free radicals in the rural North China Plain: effects on water solubility and PM_{2.5} oxidative potential

Xu Yang et al.

Correspondence to: Fobang Liu (fobang.liu@xjtu.edu.cn) and Haijie Tong (haijie.tong@hereon.de)

The copyright of individual parts of the supplement might differ from the article licence.

20 **Section S1: Methods in the quantification of PM oxidative potential**

21 **OP^{DTT}**: In the DTT depletion assay, the PM filters were first extracted using phosphate-buffered saline (PBS, pH = 7.4) at
22 2400 rpm for 30 min. The extracts were then adjusted to a final concentration of 100 µg/mL for each sample to account for a
23 non-linear effect. The PM extract was mixed with DTT (100 µM in PBS, Sigma-Aldrich) and incubated at 37 °C for 30 min.
24 At 5 min intervals, 200 µL of the mixture was transferred to react with 5, 5-dithiobis (2-nitrobenzoic acid) (DTNB, 0.24 mM,
25 Sigma-Aldrich) and tris buffer (6.45 mM with 20 mM ethylenediaminetetraacetic acid (EDTA)). The absorbance of the reaction
26 mixture at 412 nm was measured using a microplate reader (SuPerMax 3000FA, Shanghai Flash Spectrum). To obtain the
27 actual DTT consumption, the absorbance of matrix absorbance (PM and matrix) was subtracted from the final absorbance.
28 Additionally, the DTT loss in the filter blank was also subtracted from the DTT loss in the samples. All the steps were
29 performed in dark conditions.

30 The OP^{DTT} is calculated based on the residual DTT concentration in the samples at different time intervals, i.e., calculated
31 by the slope and intercept of the linear regression of the measured absorbance against time (Fang et al., 2015). Note that both
32 total OP (Total-OP) and water-soluble OP (WS-OP^{DTT}) were determined in this work. For Total-OP^{DTT} determination,
33 unfiltered PM extracts with filter punches left in the extracts were directly mixed with DTT. For WS-OP^{DTT} determination, the
34 extract was filtered through a 0.22 µm PTFE syringe filter before being mixed with DTT. The OP contribution from water-
35 insoluble PM components (WIS-OP^{DTT}) was considered as the difference between Total-OP^{DTT} and WS-OP^{DTT}.

36 **OP^{•OH}**: In the •OH production assay, a fluorescence-based method was used to measure •OH generated by PM. The same
37 extraction method as for the OP measurement was used and a final concentration of PM extract was obtained. Then, 10 mM
38 terephthalate (TPT, Thermo Scientific) and 200 µM ascorbic acid (Sigma-Aldrich) in PBS were added into the PM extract and
39 incubated at 37 °C for 120 min. The added TPT reacted with the generated •OH to form stable and strongly fluorescent

40 hydroxyterephthalic acid (2-OHTA). At specified time intervals (0, 30, 60, 70, 90, 120 min), 200 μL of the mixture was
41 transferred and mixed with 100 μL of dimethyl sulfoxide (100 mM in PBS) to quench the $\bullet\text{OH}$ formation (Son et al., 2015).
42 The fluorescent product 2-OHTA was detected at an excitation/emission wavelength of 310/425 nm using a microplate reader
43 (SuPerMax 3000FA, Shanghai Flash Spectrum).

44 The actual $\bullet\text{OH}$ generation rate was determined by subtracting the possible fluorescence from PM and matrix from the
45 final fluorescence. Moreover, the $\bullet\text{OH}$ generation by the filter blank was also corrected. The $\bullet\text{OH}$ generation rate was calculated
46 based on the determined 2-OHTA concentration at different time intervals as the formation of 2-OHTA is proportional to the
47 generation of $\bullet\text{OH}$. Calibration with 2-OHTA standard (TCI) at concentrations of 0, 2, 3, 4, 5, and 6 μM was performed daily
48 to quantify the formed 2-OHTA concentrations. The $\bullet\text{OH}$ concentration was then calculated by the following equation (1):

$$49 \quad [\bullet\text{OH}] = [2\text{-OHTA}]/y_{2\text{-OHTA}}, \quad (1)$$

50 where [2-OHTA] is the measured concentration of 2-OHTA, $y_{2\text{-OHTA}}$ is the molar yield of 2-OHTA from the reaction
51 of $\bullet\text{OH}$ with TPT in PBS, which is 0.35 at pH 7.2 (Li et al., 2019).

52 Similar to OP measurements, both the $\bullet\text{OH}$ generation rate by total PM (Total-OP^{OH}) and water-soluble PM components
53 (WS-OP^{OH}) were determined, and the same extraction method as for OP measurements was used. The $\bullet\text{OH}$ generation from
54 water-insoluble PM components (WIS-OP^{OH}) was considered as the difference between Total-OP^{OH} and WS-OP^{OH}.

55

Section S2: Discussion of OP_v and OP_m in this work and the literature

Table S3 summarizes the OP_v and OP_m of PM determined by the DTT assay in this work and the literature. Overall, the OP_v and OP_m in this work are within the range of those previously reported in North China Plain (NCP). (Liu et al., 2018) Compared with other studies in China, the OP_v for this work was found to be lower than Beijing (Lu et al., 2014), Guangzhou (Zhang Man-Man et al., 2019), but higher than Xi'an (Wang et al., 2020b), Shanghai (Lyu et al., 2018), and Nanjing (Ma et al., 2021). In addition, for this study the OP_m was lower than in other regions except Xi'an and Guangzhou, and these results suggest that there is a significant spatial variation in OP^{DTT} in Chinese cities.

Comparison with OP from several locations around the globe found that OP_v and OP_m measured in this work were higher than in Europe and the United States (Chirizzi et al., 2017; Gao et al., 2017; Clemente et al., 2023). but lower than in India and Thailand (Puthussery et al., 2020; Wang et al., 2020a). This may be attributed to the fact that India and Thailand are densely populated and heavily polluted with PM, whereas the air in Europe and the United States is relatively clean. It should be noted that the measured OP^{DTT} varied depending on the extraction method (extraction solvent and extraction time) and filtration matrix (quartz, polytetrafluoroethylene, or mixed cellulose ester), and the OP^{DTT} showed a bimodal distribution due to the variation in particle size also, which may be attributed to the particle size distribution characteristics of carbonaceous, metals.

Table S4 summarizes the OP_v and OP_m of PM quantified by •OH in this work and in the literature. Overall, the OP^{•OH} measured in this study is lower but in the same order of magnitude when compared to the OP^{•OH} of Beijing and Wangdu in China (Li et al., 2019). It is worth noting that Beijing, Wangdu, and this study were conducted in the North China Plain, but there were significant differences between the three, indicating that there are obvious spatial differences in OP^{•OH} in the North China Plain, which may be due to the different pollution sources in different places. Meanwhile, the OP_m results in this study are only higher than those of Pakistan in the United States when compared to foreign countries, suggesting that the study area contains less redox material per unit mass of PM, which may be related to the fact that the study area is rural and there are no obvious sources of pollution emissions in the surrounding area.

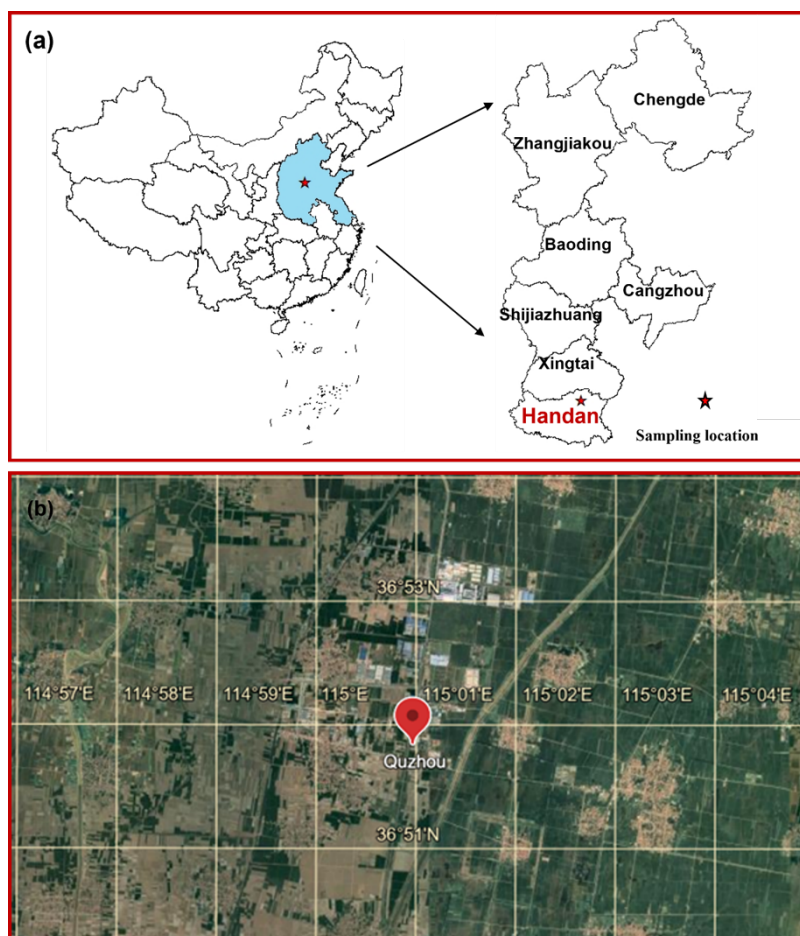


Figure S1. The location of the sampling site. (a) The Quzhou County site (the red star) in the North China Plain; (b) Specific location of the sampling site (© Google Maps).

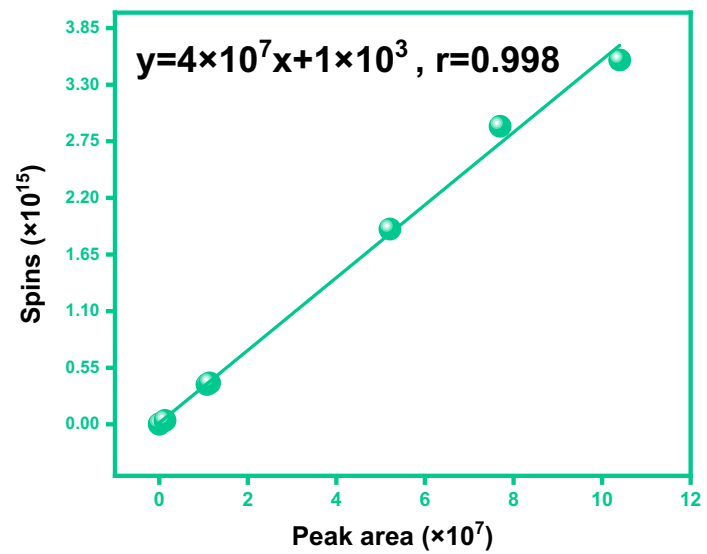


Figure S2. Calibration curve determined by peak area and spins of 4-hydroxy-2,2,6,6-tetramethylpiperidin-1-oxyl (TEMPOL).

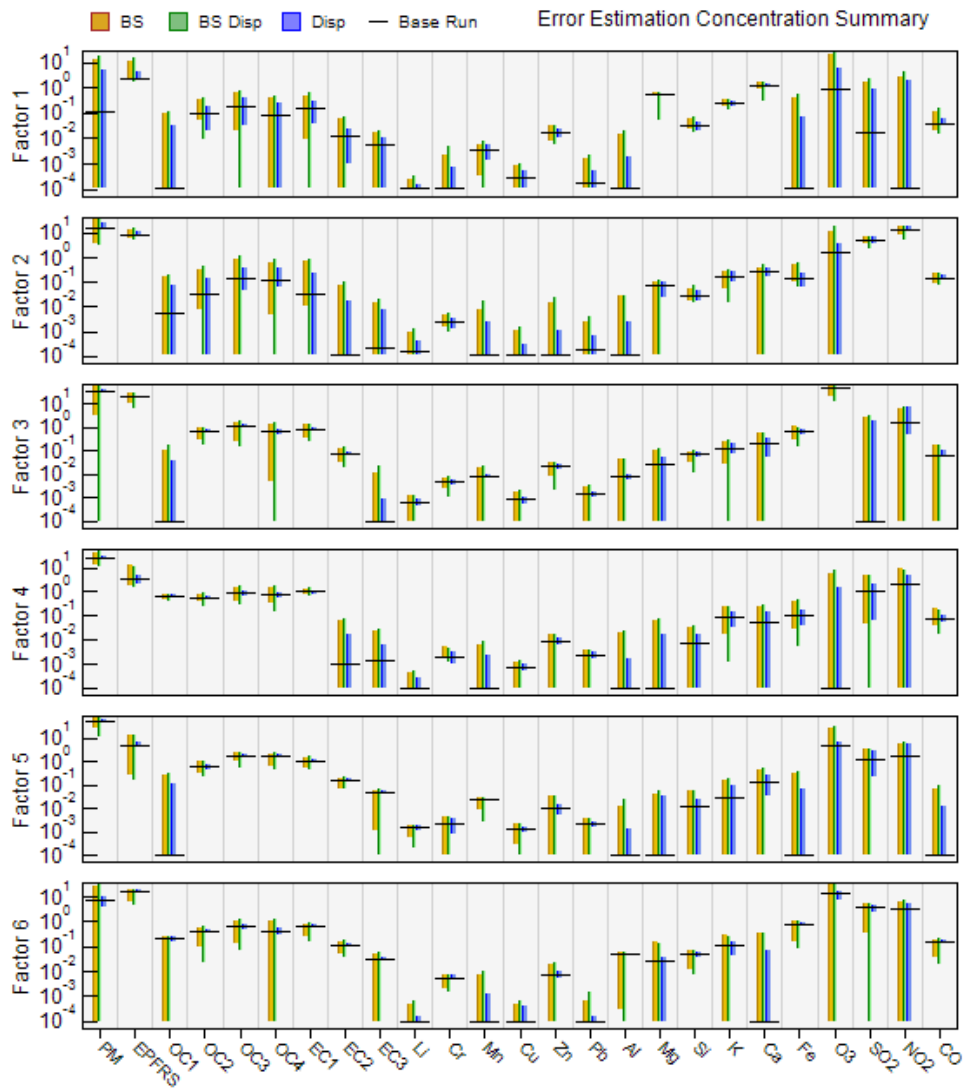


Figure S3. Summary of base run and error estimates as outputted by the PMF analysis.

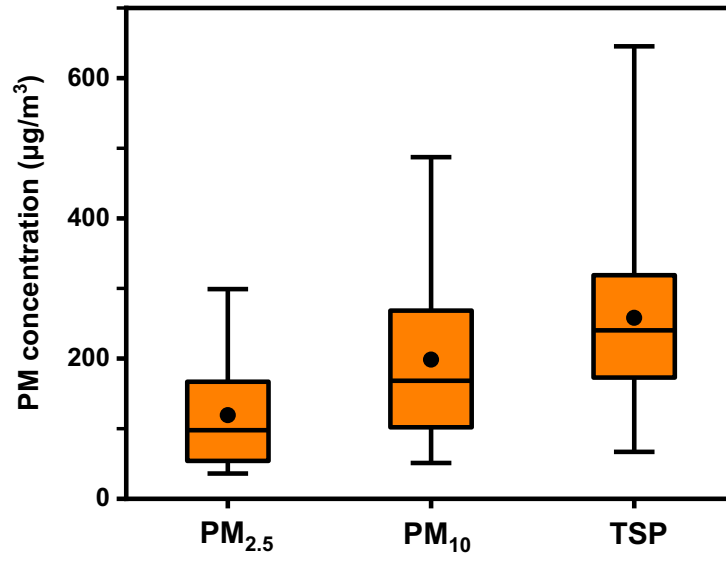


Figure S4. Box plots of PM concentrations in different particle sizes. The boxes represent the 25th percentile (lower edge), median (solid line), mean (solid dot), and 75th percentile (upper edge). The whiskers represent the minimum and maximum.

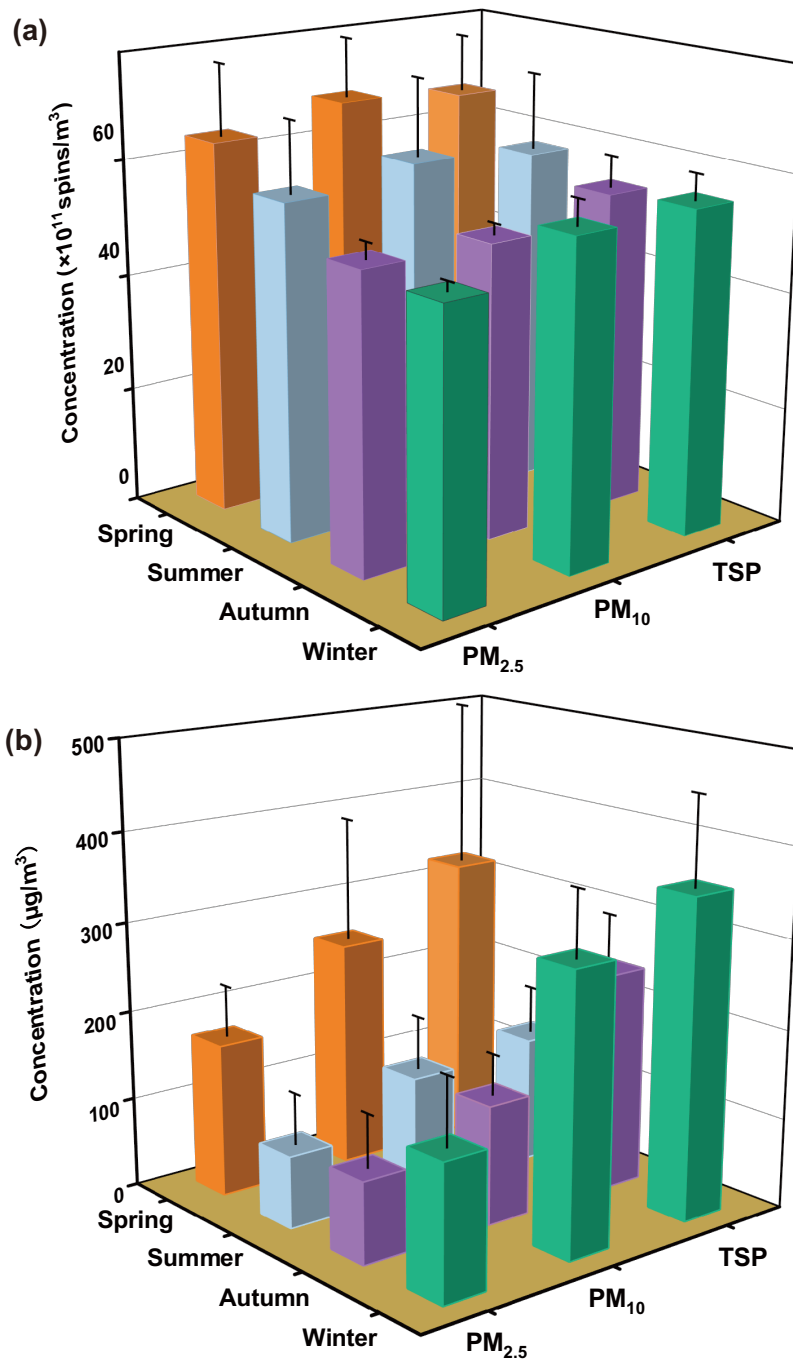


Figure S5. The concentrations of EPFRv (a) and PM (b) in different particle sizes in each season. The bars represent the standard deviations.

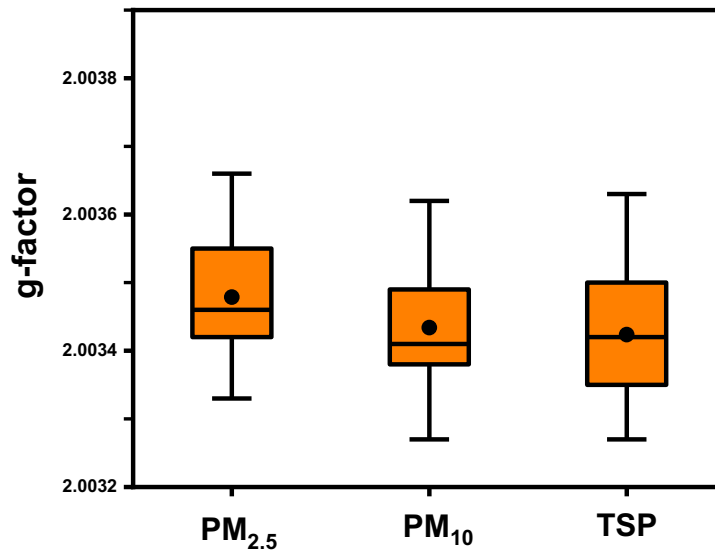


Figure S6. Box plots of variations of g-factor in different particle sizes. The boxes represent the 25th percentile (lower edge), median (solid line), mean (solid dot), and 75th percentile (upper edge). The whiskers represent the minimum and maximum.

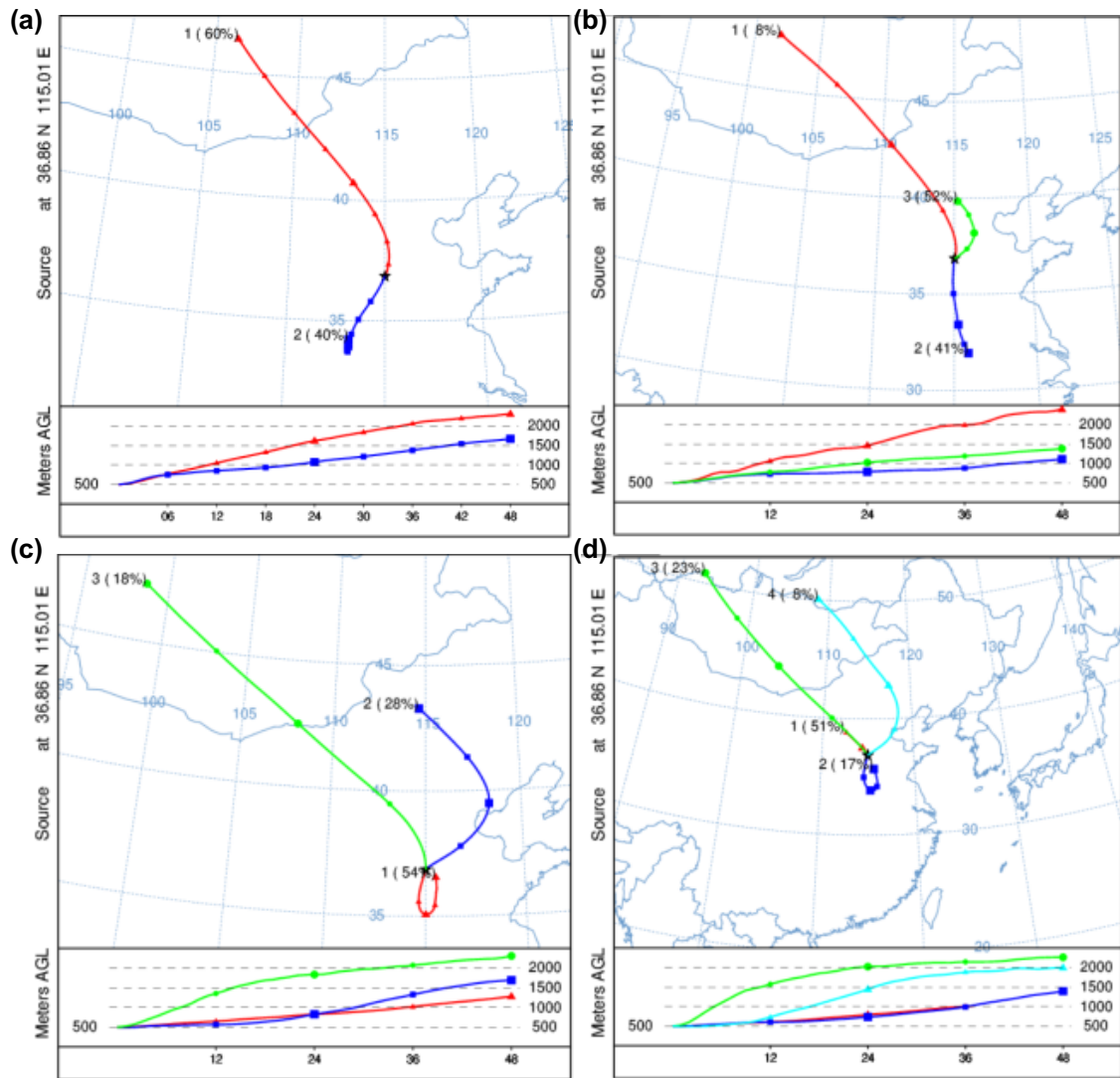


Figure S7. The 48-hr backward trajectory clusters by HYSPLIT for (a) spring; (b) summer; (c) autumn and (d) winter.

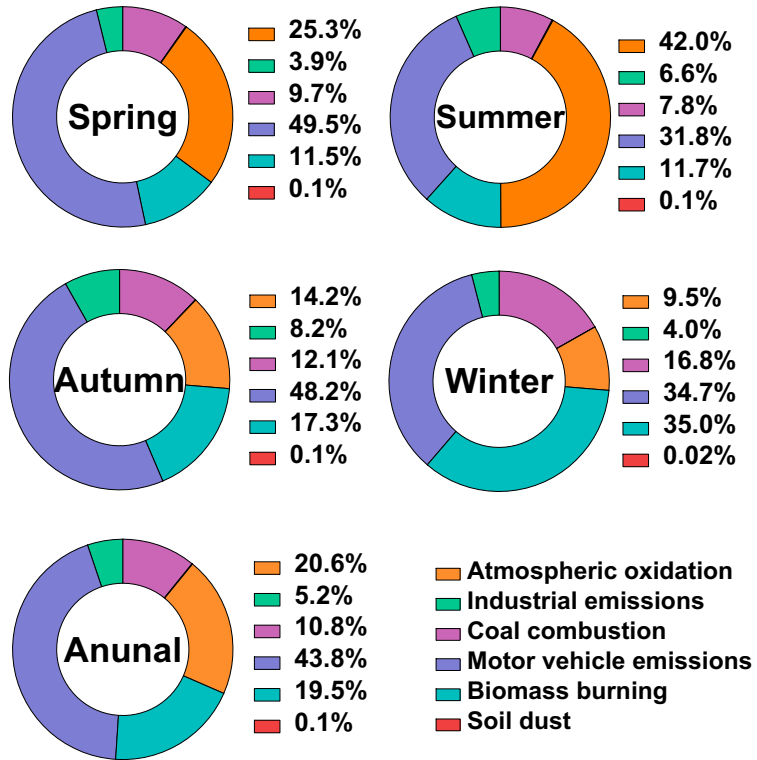


Figure S8. Seasonal and annual contributions of the six factors to PM.

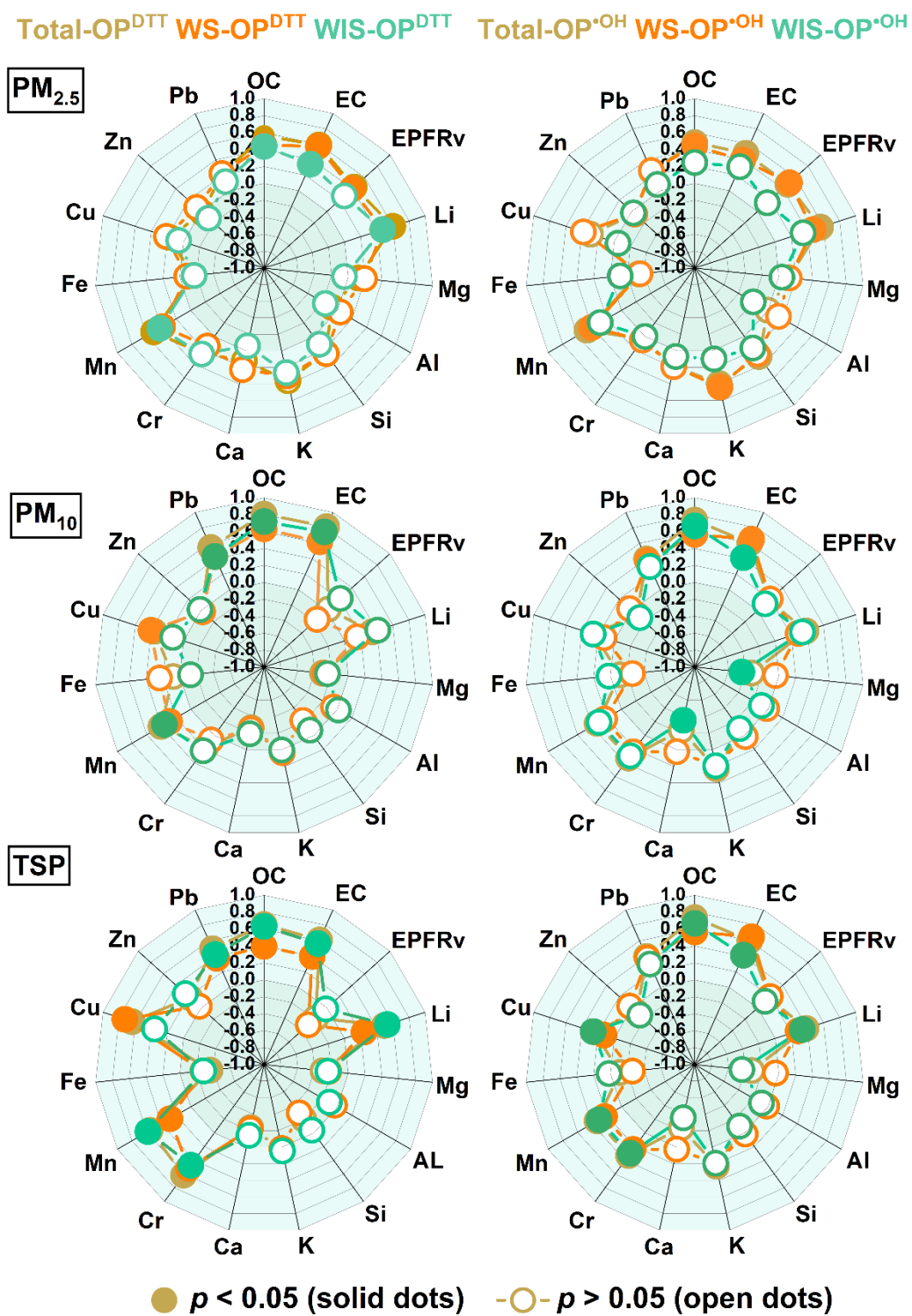


Figure S9. Correlation coefficients (Pearson's r) of volume-normalized OP (Total/WS/WIS) with selected chemical species per cubic meter of air.

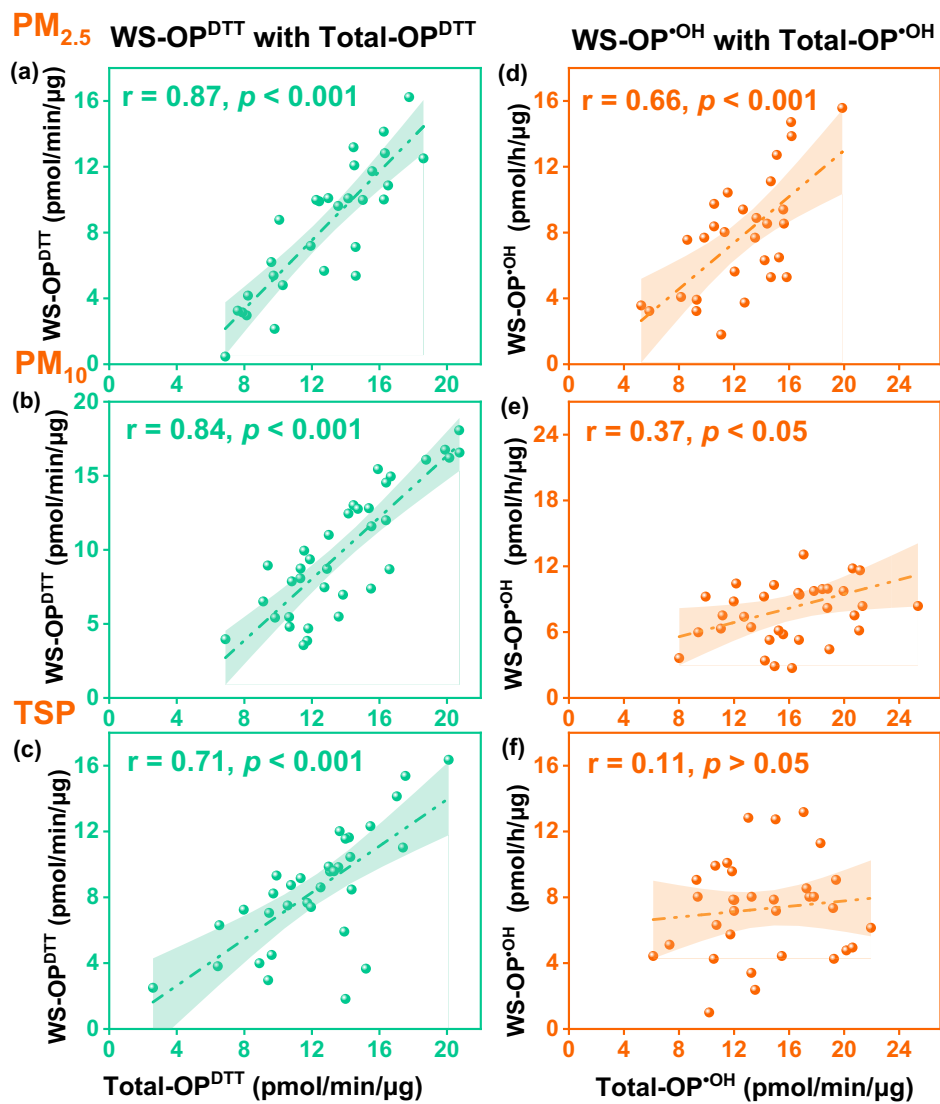


Figure S10. Correlations between WS-OP and Total-OP in different particle sizes; (a-c) Total-OP^{DTT} with WS-OP^{DTT}; (d-f) Total-OP^{OH} with WS-OP^{OH}. The Pearson correlation coefficients (r) and associated p values are illustrated in the figure. The lines and shadow areas are linear regressions with their 95% confidence intervals.

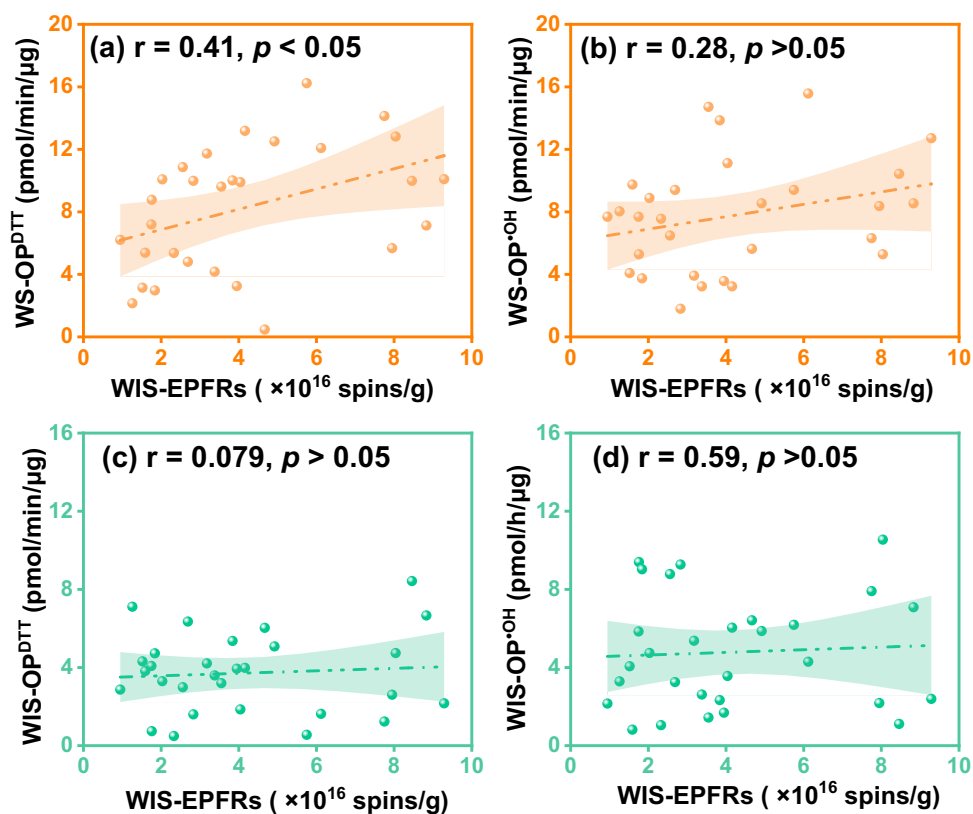


Figure S11. Correlations between WIS-EPFRs and OP; (a-b) WIS-EPFRs with OP_{WS}; (c-d) WIS-EPFRs with OP_{WIS}. The Pearson correlation coefficients (r) and associated p values are illustrated in the figure. The lines and shadow areas are linear regressions with their 95% confidence intervals.

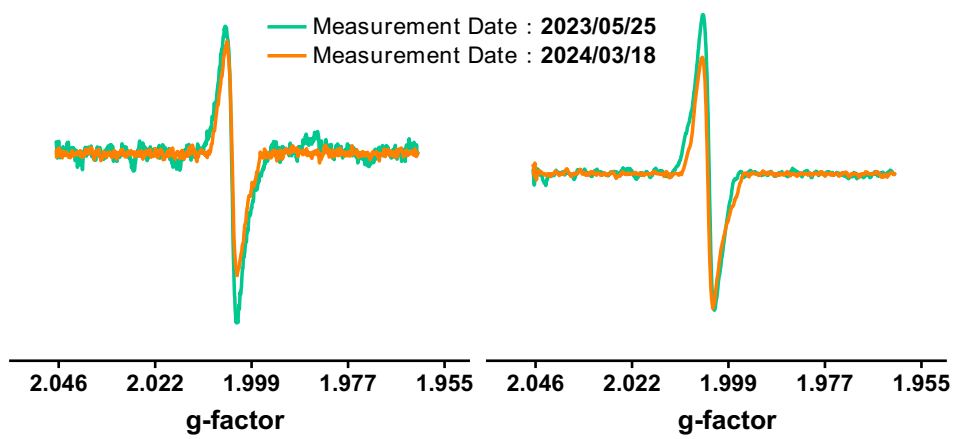


Figure S12. EPR spectra of two randomly selected PM_{2.5} samples were measured on 25 May 2023 and 18 March 2024, showing the stability of the EPFRs.

Table S1. Detailed information on the number of different size PM samples in each season

Season	Particle size	Number
Spring	PM _{2.5}	7
	PM ₁₀	8
	TSP	8
Summer	PM _{2.5}	8
	PM ₁₀	9
	TSP	9
Autumn	PM _{2.5}	8
	PM ₁₀	9
	TSP	9
Winter	PM _{2.5}	6
	PM ₁₀	7
	TSP	7

Table S2. Comparison of EPFRs in this work and the literature

Location	Type	Site type	Sampling period	PM size	EPFRm (spins/g)	EPFRv (spins/m ³)	References
Quzhou, China	Rural	Villager	2022.04 - 2023.03	PM _{2.5}	$6.48 \pm 3.53 \times 10^{16}$	$5.55 \pm 1.05 \times 10^{12}$	This study
				PM ₁₀	$3.91 \pm 2.13 \times 10^{16}$	$5.83 \pm 1.04 \times 10^{12}$	
				TSP	$2.96 \pm 1.68 \times 10^{16}$	$5.85 \pm 1.07 \times 10^{12}$	
Harbin, China	Urban	Residential, traffic, commercial	Non-heating season, 2020	Different size		4.58×10^{12}	Jia et al. (2023)
			Heating season, 2020			1.75×10^{14}	
Chongqing, China	Urban	Residential, traffic	Spring, 2017	PM _{2.5}	2.83×10^{18}	6.5×10^{13}	Qian et al. (2020)
			Summer, 2017		3.54×10^{18}	4.8×10^{13}	
			Autumn, 2017		2.50×10^{18}	8.4×10^{13}	
			Winter, 2017		1.90×10^{18}	8.1×10^{13}	
Nanjing, China	Urban	Residential, commercial	2019.03 - 2019.05	PM _{2.5}	$1.16 - 10.8 \times 10^{16}$	7.61×10^{12}	Guo et al. (2020)
Xi'an, China	Urban	Residential	Spring, 2017	PM _{2.5}	3.71×10^{15}	1.65×10^{14}	Wang et al. (2019)
			Summer, 2017		3.19×10^{15}	9.52×10^{13}	
			Autumn, 2017		1.92×10^{15}	1.04×10^{14}	
			Winter, 2017		1.84×10^{15}	1.79×10^{14}	
Yuncheng, China	Urban	Residential	Non-heating season, 2020	PM _{2.5}		12.7×10^{12}	Ai et al. (2023)
			Heating season, 2020			28.2×10^{12}	
Beijing, China	Urban	Residential	Non-heating season, 2020	PM _{2.5}		16.2×10^{12}	Ai et al. (2023)
			Heating season, 2020			14.2×10^{12}	
Beijing, China	Urban	Residential	2016.11-2016.12	TSP	$0.31 - 6.2 \times 10^{20}$	$1.6 - 4.5 \times 10^{16}$	Yang et al. (2017)
				PM _{<1}	$0.74 - 3.9 \times 10^{20}$	$2.7 - 3.5 \times 10^{16}$	
				PM _{1.0-2.5}	$0.47 - 6.5 \times 10^{20}$	$0.29 - 1.4 \times 10^{16}$	

				PM _{2.5-10}	ND - 8.2×10^{19}	$0.51 - 2.2 \times 10^{15}$	
Lahore, Pakistan	Urban	Residential	Summer, 2019	PM _{2.5}	2.3×10^{17}	1.7×10^{13}	Ahmad et al. (2023)
			Winter, 2019		1.1×10^{17}	1.2×10^{14}	
Louisiana, US	Urban		2008.10 - 2011.10	PM _{2.5}	$0.20 - 34.8 \times 10^{17}$		Gehling and Dellinger (2013)
Saudi, Arabia	Urban	Industrial, residential, and traffic	2011.10-2012.06	PM _{2.5}	$1.6 - 5.8 \times 10^{16}$		Shaltout et al. (2015)
US	Urban	Five sites		PM _{2.5}	$0.13 - 1.5 \times 10^{17}$		Squadrito et al. (2001)
Mainz, German	Suburban	Residential	2015.05-2015.07	Different size	$0.68 - 69.5 \times 10^{16}$		Arangio et al. (2016)

Table S3. The oxidative potential (OP) of PM determined by DTT assay in this work and the literature

Location	Type	Site type	Sampling period	PM size	Determined OP type	OP _v (nmol/min/m ³)	OP _m (pmol/min/μg)	References
Quzhou, China	Rural		2022.04 - 2023.03	PM _{2.5}	Total	1.35 ± 0.74	12.23 ± 3.18	This study
					Water-soluble	0.87 ± 0.51	8.51 ± 4.01	
				PM ₁₀	Total	2.78 ± 1.56	14.82 ± 3.78	
					Water-soluble	1.78 ± 0.97	10.14 ± 4.38	
				TSP	Total	3.10 ± 1.84	12.22 ± 3.60	
					Water-soluble	2.01 ± 1.07	8.44 ± 3.60	
Jinzhou, China	Urban	Educational	2015.05 - 2016.04	PM _{2.5}	Water-soluble	4.4 ± 2.6	35 ± 18	Liu et al. (2018)
Tianjin, China	Urban	Commercial				6.8 ± 3.4	49 ± 16	
Yantai, China	Urban	Residential and districts				4.2 ± 2.7	30 ± 16	
Beijing, China	Urban	Educational	2015.05 - 2016.04	PM _{2.5}	Water-soluble	12.26 ± 6.82	130 ± 100	Lu et al. (2014)
Nanjing, China	Urban	Residential and plants	2016.03 - 2016.12	PM _{2.5}	Water-soluble	1.16	20	Ma et al. (2021)
Shanghai, China	Urban	Educational	Haze periods,	Different size	Water-soluble	0.19	62.3	Lyu et al. (2018)
			Nonaze periods,			0.78	42.3	
Xi'an, China	Urban	Residential	Spring, 2017	PM _{2.5}	Water-soluble	0.53	11.72	Wang et al. (2020b)
			Summer, 2017			0.50	15.67	
			Autumn, 2017			0.40	6.94	
			Winter, 2017			0.67	6.89	
Guangzhou, China	Urban	Educational	2017.12 - 2018.01	PM _{2.5}	Water-soluble	4.67 ± 1.06	13.47 ± 3.86	Zhang Man-Man et al. (2019)
			2018.04 - 2018.05			4.45 ± 1.02	14.66 ± 4.49	

Lecce, Italy	Urban		2013 - 2016	PM _{2.5}	Water-soluble	0.29	10.3	Chirizzi et al. (2017)
				PM ₁₀		0.36	13.0	
Atlanta, US	Urban	Educational	2016.07 - 2016.08	PM _{2.5}	Water-soluble	0.20 ± 0.04		Gao et al. (2017)
		roadside			Total	0.32 ± 0.06		
					Water-soluble	0.21 ± 0.03		
					Total	0.34 ± 0.05		
Delhi, India	Urban		2015.05 - 2016.06	PM _{2.5}	Total	5.23 ± 4.6	29.4 ± 18.48	Puthussery et al. (2020)
Bangkok, Thailand	Urban	Educational	2016.01 - 2017.01	TSP	Water-soluble	2.23 ± 0.61	48.1 ± 20.8	Wang et al. (2020a)
Elche, Spain	Urban		Winter, 2021	PM ₁₀	Water-soluble	0.40 ± 0.18	18 ± 8	Clemente et al. (2023)
			Summer, 2021			0.28 ± 0.09	11 ± 4	

Table S4. The oxidative potential (OP) of PM determined by •OH production assay in this work and the literature

Location	Type	Sampling period	PM size	Determined OP type	OP _v (pmol/min/m ³)	OP _m (pmol/h/μg)	References
Quzhou, China	Rural	2022.04 - 2023.03	PM _{2.5}	Total	24.3 ± 13.4	12.5 ± 3.36	This study
				Water-soluble	15.1 ± 10.5	7.76 ± 3.59	
			PM ₁₀	Total	53.5 ± 34.9	16.0 ± 4.15	
				Water-soluble	25.2 ± 16.7	8.17 ± 3.64	
			TSP	Total	61.5 ± 37.9	14.2 ± 4.06	
				Water-soluble	28.8 ± 16.4	7.30 ± 2.94	
Beijing, China	Urban	2014.06 - 2014.07	PM _{2.5}	Water-soluble	24.67	28.8	Li et al. (2019)
Wangdu, China	Suburban		PM _{2.5}	Water-soluble	35.93	30.58	
Lahore, Pakistan	Urban	Winter, 2019	PM _{2.5}	Water-soluble	52.9	6.08	Ahmad et al. (2023)
		Summer, 2019			33.9	12.52	
Fairbanks, US	Residential area	2022.01 - 2022.02	PM _{2.5}	Total	1.40	7.14	Yang et al. (2024)
California, US	Several regions	Summer, 2019	PM _{2.5}	Total	3.9 ± 1.3	28.8 ± 6.0	Shen et al. (2022)
		Winter, 2020			6.0 ± 2.2	37.8 ± 7.8	
Delhi, Indian	Educational	2022.9.1 - 2022.9.22	PM _{2.5}	Total	6.38 ± 0.67	17.0 ± 3.7	Li et al. (2024)

Table S5. Pearson correlation coefficients for the linear regression analysis between Total-OP and mass fraction of PM species in different PM sizes

	OP ^{DTTm}				OP ^{OHm}			
	Total Size	PM _{2.5}	PM ₁₀	TSP	Total Size	PM _{2.5}	PM ₁₀	TSP
OC	0.510**	0.701**	0.390*	0.421*	0.316**	0.492**	0.189	0.447**
EC	0.551**	0.737**	0.527**	0.453**	0.234*	0.515**	0.084	0.419*
EPFRm	0.297**	0.557**	0.325	0.024	0.001	0.480**	-0.021	-0.192
Li	0.062	0.353	-0.247	0.159	0.06	0.306	-0.312	0.282
Mg	0.225	0.471*	0.36	-0.069	-0.073	0.359	-0.147	-0.301
Al	0.187	0.338	0.193	0.028	0.075	0.324	0.001	0.165
Si	0.233*	0.438*	0.297	-0.017	-0.063	0.384*	-0.029	-0.342
K	0.159	0.285	0.251	-0.043	-0.065	0.24	0.155	-0.326
Ca	0.199	0.289	0.335	-0.029	-0.01	0.351	-0.005	-0.322
Cr	0.300**	0.539**	0.146	0.226	0.061	0.369	0.071	-0.054
Mn	0.199	0.412*	-0.025	0.165	0.044	0.348	-0.364*	0.285
Fe	0.380**	0.618**	0.370*	0.181	0.083	0.474**	-0.008	0.380*
Cu	0.113	0.354	-0.047	0.174	0.108	0.545*	-0.179	0.397*
Zn	0.307**	0.381*	0.319	0.520**	0.104	0.374*	-0.079	0.11
Pb	0.317**	0.389*	0.25	0.295	0.297**	0.530**	-0.037	0.380*

* and ** indicate significant correlation at 0.05 and 0.01 level (two-tailed), respectively.

Table S6. Pearson correlation coefficients for the linear regression analysis between WS-OP and mass fraction of PM species in different PM sizes

	OP ^{DTTm}				OP ^{OHm}			
	Total Size	PM _{2.5}	PM ₁₀	TSP	Total Size	PM _{2.5}	PM ₁₀	TSP
OC	0.343**	0.526**	0.205	0.283	0.281**	0.508**	0.041	0.166
EC	0.449**	0.625**	0.397*	0.420*	0.405**	0.444*	0.388*	0.406*
EPFRm	0.320**	0.550**	0.387*	0.204	0.329**	0.428*	0.355*	0.249
Li	-0.014	0.186	-0.313	0.208	0.149	0.322	-0.011	0.2
Mg	0.302**	0.598**	0.382	0.044	0.239*	0.19	0.400*	0.143
Al	0.249*	0.427*	0.269	0.158	0.216*	0.253	0.235	0.215
Si	0.288**	0.524**	0.381*	0.144	0.267**	0.297	0.428*	0.119
K	0.213*	0.373*	0.306	0.119	0.213*	0.26	0.348*	-0.005
Ca	0.263*	0.429*	0.371*	0.047	0.260*	0.263	0.416*	0.141
Cr	0.300**	0.535**	0.207	0.304	0.165	0.114	0.201	0.288
Mn	0.189	0.343	0.036	0.178	0.14	0.2	0.026	0.265
Fe	0.423**	0.633**	0.430*	0.333	0.275**	0.386*	0.235	0.152
Cu	0.106	0.223	-0.007	0.252	0.148	0.621**	-0.19	0.237
Zn	0.335**	0.442*	0.408*	0.526**	0.183	0.168	0.288	0.311
Pb	0.325**	0.303	0.255	0.411*	0.285**	0.499**	0.063	0.256

* and ** indicate significant correlation at 0.05 and 0.01 level (two-tailed), respectively.

Table S7. Pearson correlation coefficients for the linear regression analysis between WIS-OP and mass fraction of PM species in different PM sizes

	OP ^{DTTm}				OP ^{OHm}			
	Total Size	PM _{2.5}	PM ₁₀	TSP	Total Size	PM _{2.5}	PM ₁₀	TSP
OC	0.203*	0.434**	0.256	0.18	0.08	-0.054	0.145	0.28
EC	0.068	-0.014	0.113	0.043	-0.099	0.057	-0.242	0.107
EPFRm	-0.124	-0.213	-0.208	-0.235	-0.263*	0.035	-0.314	-0.319
Li	0.101	0.185	0.214	0.093	-0.062	-0.041	-0.289	0.118
Mg	-0.181	-0.415	-0.159	-0.137	-0.263*	0.214	-0.474*	-0.358
Al	-0.148	-0.288	-0.202	-0.242	-0.099	0.072	-0.194	0.008
Si	-0.17	-0.35	-0.243	-0.21	-0.275**	0.086	-0.382*	-0.367*
K	-0.125	-0.291	-0.175	-0.233	-0.233*	-0.042	-0.143	-0.276
Ca	-0.165	-0.394	-0.162	-0.257	-0.219*	0.09	-0.349*	-0.364*
Cr	-0.065	-0.211	-0.162	-0.101	-0.073	0.303	-0.103	-0.225
Mn	-0.028	-0.03	-0.113	-0.016	-0.068	0.181	-0.372*	0.082
Fe	-0.156	-0.282	-0.217	-0.199	-0.14	0.081	-0.203	-0.054
Cu	-0.004	0.081	-0.067	-0.11	-0.014	-0.167	-0.011	0.178
Zn	-0.12	-0.275	-0.265	-0.008	-0.046	0.24	-0.321	-0.098
Pb	-0.052	0.01	-0.076	-0.151	0.059	0.004	-0.087	-0.358

* and ** indicate significant correlation at 0.05 and 0.01 level (two-tailed), respectively.

Table S8. EPFRs concentrations (spins/m³) in original and washed samples and proportion of water-soluble fraction

Date	Particle size	Original samples	Washed samples	Water soluble fraction (%)
2022/04/08	PM _{2.5}	5.73×10^{12}	3.67×10^{12}	36.0
2022/04/15	PM _{2.5}	7.43×10^{12}	5.28×10^{12}	28.9
2022/04/23	PM _{2.5}	6.22×10^{12}	4.15×10^{12}	33.3
2022/05/18	PM _{2.5}	1.13×10^{12}	5.17×10^{12}	54.1
2022/06/02	PM _{2.5}	6.11×10^{12}	3.76×10^{12}	38.5
2022/06/15	PM _{2.5}	6.19×10^{12}	2.07×10^{12}	66.6
2022/06/23	PM _{2.5}	4.46×10^{12}	3.39×10^{12}	23.9
2022/07/2	PM _{2.5}	1.02×10^{12}	7.30×10^{12}	28.2
2022/07/17	PM _{2.5}	5.16×10^{12}	2.91×10^{12}	43.6
2022/07/23	PM _{2.5}	2.06×10^{12}	1.11×10^{12}	45.8
2022/08/1	PM _{2.5}	2.59×10^{12}	1.44×10^{12}	44.3
2022/08/22	PM _{2.5}	3.15×10^{12}	2.34×10^{12}	25.7
2022/09/01	PM _{2.5}	3.49×10^{12}	2.61×10^{12}	25.1
2022/09/16	PM _{2.5}	6.12×10^{12}	3.46×10^{12}	43.5
2022/09/22	PM _{2.5}	4.14×10^{12}	3.73×10^{12}	9.9
2022/10/04	PM _{2.5}	9.85×10^{12}	6.17×10^{12}	37.3
2022/10/12	PM _{2.5}	1.77×10^{12}	1.33×10^{12}	25.0
2022/10/21	PM _{2.5}	1.86×10^{12}	1.23×10^{12}	33.7
2022/11/03	PM _{2.5}	7.37×10^{12}	6.14×10^{12}	16.7
2022/11/12	PM _{2.5}	7.81×10^{12}	6.77×10^{12}	13.3
2022/12/07	PM _{2.5}	4.64×10^{12}	3.32×10^{12}	28.4
2022/12/25	PM _{2.5}	3.95×10^{12}	1.86×10^{12}	52.9
2023/01/02	PM _{2.5}	7.46×10^{12}	3.34×10^{12}	55.2
2023/01/25	PM _{2.5}	9.41×10^{12}	6.21×10^{12}	34.0
2023/02/15	PM _{2.5}	7.73×10^{12}	4.36×10^{12}	43.6
2023/02/25	PM _{2.5}	8.64×10^{11}	8.16×10^{12}	5.6
2023/03/5	PM _{2.5}	1.17×10^{12}	8.05×10^{121}	31.5
2023/03/12	PM _{2.5}	1.71×10^{12}	1.30×10^{12}	24.4
2023/03/27	PM _{2.5}	3.04×10^{12}	2.37×10^{12}	21.9
2022/04/24	PM ₁₀	5.62×10^{12}	4.35×10^{12}	22.6
2023/03/13	PM ₁₀	1.82×10^{12}	1.06×10^{12}	41.5
2022/04/17	TSP	1.00×10^{12}	5.69×10^{12}	43.2
2023/03/29	TSP	1.37×10^{12}	5.66×10^{12}	58.8
2022/06/03	PM ₁₀	1.39×10^{12}	9.78×10^{11}	29.7
2022/07/18	PM ₁₀	4.99×10^{12}	3.22×10^{12}	35.4
2022/06/04	TSP	1.45×10^{12}	8.63×10^{11}	40.5
2022/06/18	TSP	9.73×10^{12}	8.05×10^{12}	17.2
2022/10/22	PM ₁₀	1.27×10^{12}	9.55×10^{11}	24.5
2022/11/27	PM ₁₀	2.06×10^{12}	1.42×10^{12}	31.4

2022/10/06	TSP	4.73×10^{12}	2.68×10^{12}	43.4
2022/10/24	TSP	1.78×10^{12}	1.10×10^{12}	38.2
2023/01/26	PM ₁₀	2.25×10^{12}	1.60×10^{12}	28.9
2023/02/06	PM ₁₀	1.65×10^{12}	8.60×10^{11}	47.9
2022/12/27	TSP	2.40×10^{12}	1.07×10^{12}	55.4
2023/02/07	TSP	4.68×10^{12}	2.64×10^{12}	43.6
Average				35.2

Table S9. EPFRs concentrations (spins/m³) in original and acidified samples and proportion of acid-reduced fraction

Date	Particle size	Original samples	Acidified samples	Acid-reduced fraction (%)
2022/04/08	PM _{2.5}	3.99×10^{12}	1.74×10^{12}	56.5
2022/07/23	PM _{2.5}	1.51×10^{12}	6.21×10^{12}	58.8
2022/08/22	PM _{2.5}	3.16×10^{12}	9.65×10^{12}	69.4
2022/07/17	PM _{2.5}	2.28×10^{12}	1.03×10^{12}	54.5
2023/03/05	PM _{2.5}	4.49×10^{12}	ND	100
2023/03/12	PM _{2.5}	1.86×10^{12}	4.08×10^{11}	78.1
Average				69.6

Table S10. Pearson correlation coefficients between EPFRm and mass fraction of PM species

	Total Size	PM _{2.5}	PM ₁₀	TSP
OC	0.463**	0.694**	0.133	0.023
EC	0.630**	0.784**	0.284	0.286
Li	0.114	0.249	0.132	0.091
Mg	0.705**	0.658**	0.569**	0.593**
Al	0.575**	0.490**	0.741**	0.420*
Si	0.919**	0.876**	0.936**	0.894**
K	0.774**	0.809**	0.680**	0.308
Ca	0.623**	0.560**	0.614**	0.362*
Cr	0.793**	0.781**	0.681**	0.693**
Mn	0.348**	0.405*	0.357*	0.078
Fe	0.880**	0.951**	0.814**	0.693**
Cu	0.101	0.269	-0.049	-0.369*
Zn	0.536**	0.489**	0.778**	0.472**
Pb	0.187	0.411*	0.117	0.097

* and ** indicate significant correlation at 0.05 and 0.01 level (two-tailed), respectively.

References

- Ahmad, M., Chen, J., Yu, Q., Tariq Khan, M., Weqas Ali, S., Nawab, A., Phairuang, W., and Panyametheekul, S.: Characteristics and Risk Assessment of Environmentally Persistent Free Radicals (EPFRs) of PM_{2.5} in Lahore, Pakistan, *Int. J. Environ. Res. Public Health.*, 20, 2384, <https://doi.org/10.3390/ijerph20032384>, 2023.
- Ai, J., Qin, W. H., Chen, J., Sun, Y. W., Yu, Q., Xin, K., Huang, H. Y., Zhang, L. Y., Ahmad, M., and Liu, X. A.: Pollution characteristics and light-driven evolution of environmentally persistent free radicals in PM_{2.5} in two typical northern cities of China, *J. Hazard. Mater.*, 454, 131466, <https://doi.org/10.1016/j.jhazmat.2023.131466>, 2023.
- Arangio, A. M., Tong, H. J., Socorro, J., Pöschl, U., and Shiraiwa, M.: Quantification of environmentally persistent free radicals and reactive oxygen species in atmospheric aerosol particles, *Atmos. Chem. Phys.*, 16, 13105-13119, <https://doi.org/10.5194/acp-16-13105-2016>, 2016.
- Chirizzi, D., Cesari, D., Guascito, M. R., Dinoi, A., Giotta, L., Donateo, A., and Contini, D.: Influence of Saharan dust outbreaks and carbon content on oxidative potential of water-soluble fractions of PM_{2.5} and PM₁₀, *Atmos. Environ.*, 163, 1-8, <https://doi.org/10.1016/j.atmosenv.2017.05.021>, 2017.
- Clemente, A., Gil-Moltó, J., Yubero, E., Juárez, N., Nicolás, J. F., Crespo, J., and Galindo, N.: Sensitivity of PM₁₀ oxidative potential to aerosol chemical composition at a Mediterranean urban site: ascorbic acid versus dithiothreitol measurements, *Air Qual. Atmos. Health.*, 16, 1165-1172, <https://doi.org/10.1007/s11869-023-01332-1>, 2023.
- Fang, T., Verma, V., Guo, H., King, L. E., and Edgerton, E. S.: A semi-automated system for quantifying the oxidative potential of ambient particles in aqueous extracts using the dithiothreitol (DTT) assay: results from the Southeastern Center for Air Pollution and Epidemiology (SCAPE), *Atmos. Meas. Tech.*, 8, 471-482, <https://doi.org/10.5194/amt-8-471-2015>, 2015.
- Gao, D., Fang, T., Verma, V., Zeng, L. G., and Weber, R. J.: A method for measuring total aerosol oxidative potential (OP) with the dithiothreitol (DTT) assay and comparisons between an urban and roadside site of water-soluble and total OP, *Atmos. Meas. Tech.*, 10, 2821-2835, <https://doi.org/10.5194/amt-10-2821-2017>, 2017.
- Gehling, W. and Dellinger, B.: Environmentally Persistent Free Radicals and Their Lifetimes in PM_{2.5}, *Environ. Sci. Technol.*, 47, 8172-8178, <https://doi.org/10.1021/es401767m>, 2013.
- Guo, X. W., Zhang, N., Hu, X., Huang, Y., Ding, Z. H., Chen, Y. J., and Lian, H. Z.: Characteristics and potential inhalation exposure risks of PM_{2.5} - bound environmental persistent free radicals in Nanjing, a mega-city in China, *Atmos. Environ.*, 224, 117355, <https://doi.org/10.1016/j.atmosenv.2020.117355>, 2020.
- Jia, S.-M., Wang, D.-Q., Liu, L.-Y., Zhang, Z.-F., and Ma, W.-L.: Size-resolved environmentally persistent free radicals in cold region atmosphere: Implications for inhalation exposure risk, *J. Hazard. Mater.*, 443, 130263, <https://doi.org/10.1016/j.jhazmat.2022.130263>, 2023.
- Li, C., Hakkim, H., Sinha, V., Sinha, B., Pardo, M., Cai, D., Reicher, N., Chen, J., Hao, K., and Rudich, Y.: Variation of PM_{2.5} Redox Potential and Toxicity During Monsoon in Delhi, India, *ACS ES&T Air.*, 1, 316-329, <https://doi.org/10.1021/acsestair.3c00096>, 2024.
- Li, X. Y., Kuang, X. B. M., Yan, C. Q., Ma, S. X., Paulson, S. E., Zhu, T., Zhang, Y. H., and Zheng, M.: Oxidative Potential by PM_{2.5} in the North China Plain: Generation of Hydroxyl Radical, *Environ. Sci. Technol.*, 53, 512-520, <https://doi.org/10.1021/acs.est.8b05253>, 2019.
- Liu, W. J., Xu, Y. S., Liu, W. X., Liu, Q. Y., Yu, S. Y., Liu, Y., Wang, X., and Tao, S.: Oxidative potential of ambient PM_{2.5} in the coastal cities of the Bohai Sea, northern China: Seasonal variation and source apportionment, *Environ. Pollut.*, 236, 514-528, <https://doi.org/10.1016/j.envpol.2018.01.116>, 2018.
- Lu, Y., Su, S., Jin, W. J., Wang, B., Li, N., Shen, H. Z., Li, W., Huang, Y., Chen, H., Zhang, Y. Y., Chen, Y. C., Lin,

N., Wang, X. L., and Tao, S.: Characteristics and cellular effects of ambient particulate matter from Beijing, *Environ. Pollut.*, 191, 63-69, <https://doi.org/10.1016/j.envpol.2014.04.008>, 2014.

Lyu, Y., Guo, H. B., Cheng, T. T., and Li, X.: Particle Size Distributions of Oxidative Potential of Lung-Deposited Particles: Assessing Contributions from Quinones and Water-Soluble Metals, *Environ. Sci. Technol.*, 52, 6592-6600, <https://doi.org/10.1021/acs.est.7b06686>, 2018.

Ma, X. Y., Nie, D. Y., Chen, M. D., Ge, P. X., Liu, Z. J., Ge, X. L., Li, Z. R., and Gu, R.: The Relative Contributions of Different Chemical Components to the Oxidative Potential of Ambient Fine Particles in Nanjing Area, *Int. J. Environ. Res. Public Health.*, 18, 17, <https://doi.org/10.3390/ijerph18062789>, 2021.

Puthussery, J. V., Singh, A., Rai, P., Bhattu, D., Kumar, V., Vats, P., Furger, M., Rastogi, N., Slowik, J. G., Ganguly, D., Prevot, A. S. H., Tripathi, S. N., and Verma, V.: Real-Time Measurements of PM_{2.5} Oxidative Potential Using a Dithiothreitol Assay in Delhi, India, *Environ. Sci. Technol. Lett.*, 7, 504-510, <https://doi.org/10.1021/acs.estlett.0c00342>, 2020.

Qian, R. Z., Zhang, S. M., Peng, C., Zhang, L. Y., Yang, F. M., Tian, M., Huang, R. J., Wang, Q. Y., Chen, Q. C., Yao, X. J., and Chen, Y.: Characteristics and potential exposure risks of environmentally persistent free radicals in PM_{2.5} in the three gorges reservoir area, Southwestern China, *Chemosphere.*, 252, 10, <https://doi.org/10.1016/j.chemosphere.2020.126425>, 2020.

Shaltout, A. A., Boman, J., Shehadeh, Z. F., Al-Malawi, D. A. R., Hemed, O. M., and Morsy, M. M.: Spectroscopic investigation of PM_{2.5} collected at industrial, residential and traffic sites in Taif, Saudi Arabia, *J. Aerosol Sci.*, 79, 97-108, <https://doi.org/10.1016/j.jaerosci.2014.09.004>, 2015.

Shen, J. Q., Taghvaei, S., La, C., Oroumijeh, F., Liu, J., Jerrett, M., Weichenthal, S., Del Rosario, I., Shafer, M. M., Ritz, B., Zhu, Y. F., and Paulson, S. E.: Aerosol Oxidative Potential in the Greater Los Angeles Area: Source Apportionment and Associations with Socioeconomic Position, *Environ. Sci. Technol.*, 56, 17795-17804, <https://doi.org/10.1021/acs.est.2c02788>, 2022.

Son, Y., Mishin, V., Welsh, W., Lu, S. E., Laskin, J. D., Kipen, H., and Meng, Q. M.: A Novel High-Throughput Approach to Measure Hydroxyl Radicals Induced by Airborne Particulate Matter, *Int. J. Environ. Res. Public Health.*, 12, 13678-13695, <https://doi.org/10.3390/ijerph121113678>, 2015.

Squadrito, G. L., Cueto, R., Dellinger, B., and Pryor, W. A.: Quinoid redox cycling as a mechanism for sustained free radical generation by inhaled airborne particulate matter, *Free Radical Biol. Med.*, 31, 1132-1138, [https://doi.org/10.1016/s0891-5849\(01\)00703-1](https://doi.org/10.1016/s0891-5849(01)00703-1), 2001.

Wang, J. Q., Jiang, H. Y., Jiang, H. X., Mo, Y. Z., Geng, X. F., Li, J. B., Mao, S. D., Bualert, S., Ma, S. X., Li, J., and Zhang, G.: Source apportionment of water-soluble oxidative potential in ambient total suspended particulate from Bangkok: Biomass burning versus fossil fuel combustion, *Atmos. Environ.*, 235, 117624, <https://doi.org/10.1016/j.atmosenv.2020.117624>, 2020a.

Wang, Y. Q., Li, S. P., Wang, M. M., Sun, H. Y., Mu, Z., Zhang, L. X., Li, Y. G., and Chen, Q. C.: Source apportionment of environmentally persistent free radicals (EPFRs) in PM_{2.5} over Xi'an, China, *Sci. Total Environ.*, 689, 193-202, <https://doi.org/10.1016/j.scitotenv.2019.06.424>, 2019.

Wang, Y. Q., Wang, M. M., Li, S. P., Sun, H. Y., Mu, Z., Zhang, L. X., Li, Y. G., and Chen, Q. C.: Study on the oxidation potential of the water-soluble components of ambient PM_{2.5} over Xi'an, China: Pollution levels, source apportionment and transport pathways, *Environ. Int.*, 136, 11, <https://doi.org/10.1016/j.envint.2020.105515>, 2020b.

Yang, L. L., Liu, G. R., Zheng, M. H., Jin, R., Zhu, Q. Q., Zhao, Y. Y., Wu, X. L., and Xu, Y.: Highly Elevated Levels and Particle-Size Distributions of Environmentally Persistent Free Radicals in Haze-Associated Atmosphere, *Environ. Sci. Technol.*, 51, 7936-7944, <https://doi.org/10.1021/acs.est.7b01929>, 2017.

Yang, Y., Battaglia, M. A., Mohan, M. K., Robinson, E. S., DeCarlo, P. F., Edwards, K. C., Fang, T., Kapur, S.,

Shiraiwa, M., Cesler-Maloney, M., Simpson, W. R., Campbell, J. R., Nenes, A., Mao, J., and Weber, R. J.: Assessing the Oxidative Potential of Outdoor PM_{2.5} in Wintertime Fairbanks, Alaska, ACS ES&T Air, 1, 175-187, <https://doi.org/10.1021/acsestair.3c00066>, 2024.

Zhang Man-man, LI Hui-rong, Yang Wen-da, Sun Jia-yin, and Cheng, W.: Measurement based on DTT method of the PM_{2.5} oxidative potential in Guangzhou urban area, China Environ. Sci.2019.